Eur. Phys. J. B (2015) 88: 135
DOI: 10.1140/epjb/e2015-50850-x

THE EUROPEAN PHYSICAL JOURNAL B

Regular Article

Temperature and strain-rate effects on the deformation behaviors of nano-crystalline graphene sheets

Zhi Yang[1], Yuhong Huang[2], Fei Ma[1,3,a], Yunjin Sun[4], Kewei Xu[1,5,b], and Paul K. Chu[3,c]

[1] State Key Laboratory for Mechanical Behavior of Materials, Xi'an Jiaotong University, Xi'an 710049, Shaanxi, P.R. China
[2] College of Physics and Information Technology, Shaanxi Normal University, Xi'an 710062, Shaanxi, P.R. China
[3] Department of Physics and Materials Science, City University of Hong Kong, Tat Chee Avenue, Kowloon, Hong Kong, P.R. China
[4] Faculty of Food Science and Engineering, Beijing University of Agriculture Beijing Key Laboratory of Agricultural Product Detection and Control of Spoilage Organisms and Pesticide Residue, Beijing Laboratory of Food Quality and Safety, Beijing 102206, P.R. China
[5] Department of Physics and Opt-electronic Engineering, Xi'an University of Arts and Science, Xi'an 710065, Shaanxi, P.R. China

Received 10 December 2014 / Received in final form 14 April 2015
Published online 27 May 2015 –

Abstract. The deformation behavior of nanocrystalline graphene sheets is investigated by molecular dynamics (MD) simulation by coupling the effects of the temperature and strain rate. Mechanical deformation of graphene sheets, which is dominated by the competition between bond breaking and rotation, is essentially an atomic behavior. Similar to single-crystal graphene sheets, nanocrystalline graphene sheets usually exhibit bond breaking induced brittle fracture along grain boundaries after large elastic deformation. The elastic modulus decreases slightly with temperature as a result of softening but does not depend on the strain rate. A brittle-plastic transition by bond rotation and rearrangement under stress appears to occur at high temperature above 1000 K, but the ductility is unexpectedly reduced due to accelerated bond breaking. At small strain rates, it is easier for bonds to rearrange, vacancies to coalesce, and cracks to propagate in grain boundaries and plastic deformation with a larger activation volume occurs. However, at large strain rates, the relaxation time is too short for atomic bonds to rotate and rearrange under stress. Therefore, bond elongation and brittle fracture with a smaller activation volume takes place. The results demonstrate that the atomic behavior in grain boundaries is crucial to mechanical deformation in nanocrystalline graphene sheets, which is temperature and strain rate sensitive.

1 Introduction

Graphene is a single layer of sp^2 hybridized carbon atoms in a honeycomb two-dimensional (2D) lattice in which each carbon atom is bonded to three adjacent atoms via C-C covalent bonds. The left P_z orbits perpendicular to sp^2 counterparts lead to the delocalized π bonds. As a result, graphene possesses the unique properties of ultra-low resistivity down to 1.0 $\mu\,\Omega\,$cm [1], high carrier mobility in excess of 200 000 $\mathrm{cm}^2/(\mathrm{V\,s})$ [2], high thermal conductivity over 5000 $\mathrm{W/(m\,K)}$ at room temperature [3], high strength [4,5], excellent flexibility [6,7], and high visible-light transmittance [8] thereby spurring many new applications pertaining to field effect transistors [9], foldable displays [10], touchscreens [11] and flexible energy storage devices [12]. The stability and reliability of the devices are closely related to the mechanical properties of graphene sheets. It has been illustrated that graphene sheets have large in-plane Young's modulus of 1.0 TPa and intrinsic tensile strength of 130 GPa [4,5]. Furthermore, graphene sheets exhibit a reversible hexagonal-to-orthorhombic phase transformation via lattice shearing when they are subjected to tensile loading and unloading along some directions, resulting in excellent ductility with a strain up to 35% [13]. High strength and excellent toughness, which are normally two conflicting mechanical properties of conventional materials, may be achieved from this 2D system [14]. Graphene is also believed to be an ideal reinforcing component in composite materials [15] and so it is fundamentally important to study the deformation behaviors and mechanical properties in addition to the popular optical and electronic properties.

Grantab et al. [16] have found that graphene with large-angle tilt grain boundaries is as strong as the pristine one and unexpectedly much stronger than that with low-angle grain boundaries, because the large-angle grain

[a] e-mail: mafei@mail.xjtu.edu.cn
[b] e-mail: kwxu@mail.xjtu.edu.cn
[c] e-mail: paul.chu@cityu.edu.hk

boundaries can better accommodate the strained carbon rings by in-plane bond rotation. This is impossible in bulk metals thus indicating a special deformation mechanism in the 2D materials. In essence, deformation of graphene sheets is dominated by the competition between bond breaking and bond rotation [17], which are completely atomic and sensitive to the temperature and strain rate. The tensile fracture strain varies linearly with temperature but logarithmically with the strain rate as predicted by the transition state theory [18]. The tensile strength of armchair graphene nanoribbons decreases from 95 GPa to 40 GPa by 58% when the temperature rises from 300 K to 2400 K [19], whereas the shear strength diminishes from 60 GPa to 20 GPa by 67% as the temperature goes up from 100 K to 2000 K [20]. Most of the previous investigations of the temperature effects focus on the ideal models of single-crystal or bi-crystal graphene sheets. In practice, graphene sheets are usually polycrystalline, as confirmed by high-resolution transmission microscopy (HR-TEM) and scanning tunneling microscopy (STM) [21–23] and the randomly distributed grain boundaries render the deformation behavior more complicated, especially in nanocrystalline sheets. Grain boundaries in graphene sheets are considered as an array of Stone-Wales (SW) topological defects and the carbon atoms are connected by strong covalent bonds [22,24]. Hence, deformation is dominated by the breaking, rotation, and rearrangement of covalent bonds rather than the plane slip and rotation of grains in nanocrystalline metals. In a previous work, it is found that the grain boundaries (GBs) become a principal component in two-dimensional materials with nano-grains, and the nanocrystalline graphene can be considered as a composite structure with grain domains and GBs as the two component phases. The bond length in GBs tends to be homogeneously distributed under tensile loading. This is almost the same for all the samples. Hence, the fracture stress and strain are almost size independent. The GBs have lower elastic modulus due to longer bond length and the GBs increase with reducing grain size. As a result, the elastic modulus decreases with grain size. The size-independent fracture strength and size-dependent elastic modulus are completely different from those evidenced in nanocrystalline metals. The difference can be ascribed to the remarkable atomic behaviors in the grain boundaries of nanocrystalline graphene sheets. The atomic behaviors should be sensitive to the strain rate and temperature. To this end, the strain rate and temperature sensitivity is studied in this paper.

2 Models and simulation methods

According to atomic structures revealed by experiments [21–23], the simulation models of nanocrystalline graphene sheets with randomly distributed grain size and orientation are constructed by Voronoi tessellation [20]. A Voronoi tessellation is a collection of convex polygons isolated by planar cell walls perpendicular to the lines connecting neighboring points. Each convex polygon represents a grain domain in which both the nucleation center and crystal orientation are randomly selected and the atoms are filled, accordingly. The atomically thick layers adjacent to the planar cell walls are defined as grain boundaries. The initial carbon-carbon bond length is 1.42 Å. Figure 1 displays one of the typical atomic models of the nanocrystalline graphene sheets. The color of the atoms is according to the potential energy and grain boundaries with higher potential energies are evident. In each model, $N \times N$ ($N = 3, 5, 9$) grains are in a graphene sheet with a constant simulation size of 18.5 nm×18.5 nm, corresponding to the average grain sizes of 6.17 nm, 3.7 nm, 2.06 nm, respectively. For each tensile test, three models are built to avoid accidental errors.

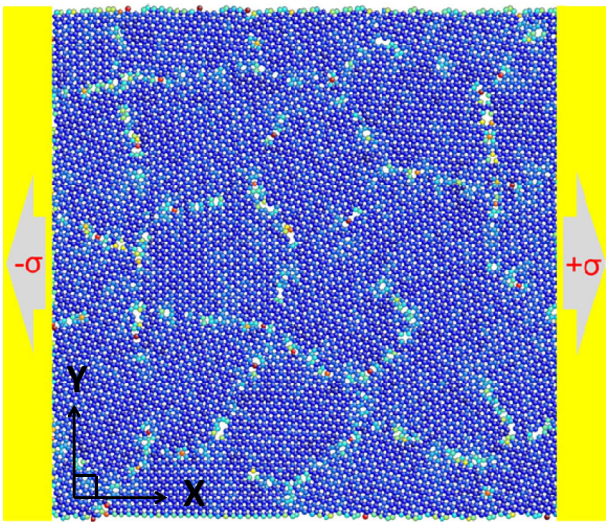

Fig. 1. Simulation model of a nanocrystalline graphene sheet under tensile loading.

The simulation is conducted using the package LAMMPS. The interactions between carbon atoms are described by AIREBO potential which can accurately capture the interaction between carbon atoms as well as bond breaking and bond reforming [25]. The cutoff parameter describing the short-range C-C interaction is selected to be 2.0 Å in order to avoid spuriously high bond forces and nonphysical results at large deformation [26]. Prior to dynamic simulation, the nanocrystalline graphene sheets are fully relaxed to an equilibrium state in the isothermal-isobaric ensemble at a given temperature. Uniaxial tensile loading is then applied along the x axis by the deformation-control method and periodic boundary conditions are adopted along the two in-plane directions. The nominal strain ε_i and nominal stress σ_i $(i = x, y)$ are defined as [27]:

$$\varepsilon_i = \frac{l_i - l_i^0}{l_i^0}, \quad \sigma_i = \frac{1}{V^0}\frac{\partial U}{\partial \varepsilon_i}, \tag{1}$$

where l_i^0 is the initial length of the nanocrystalline graphene sheets along the i $(i = x, y)$ directions, l_i is the length under stress, U is the strain energy, and V^0 is the initial volume. The interlayer separation of graphite of 3.4 Å is taken as the effective thickness of the graphene

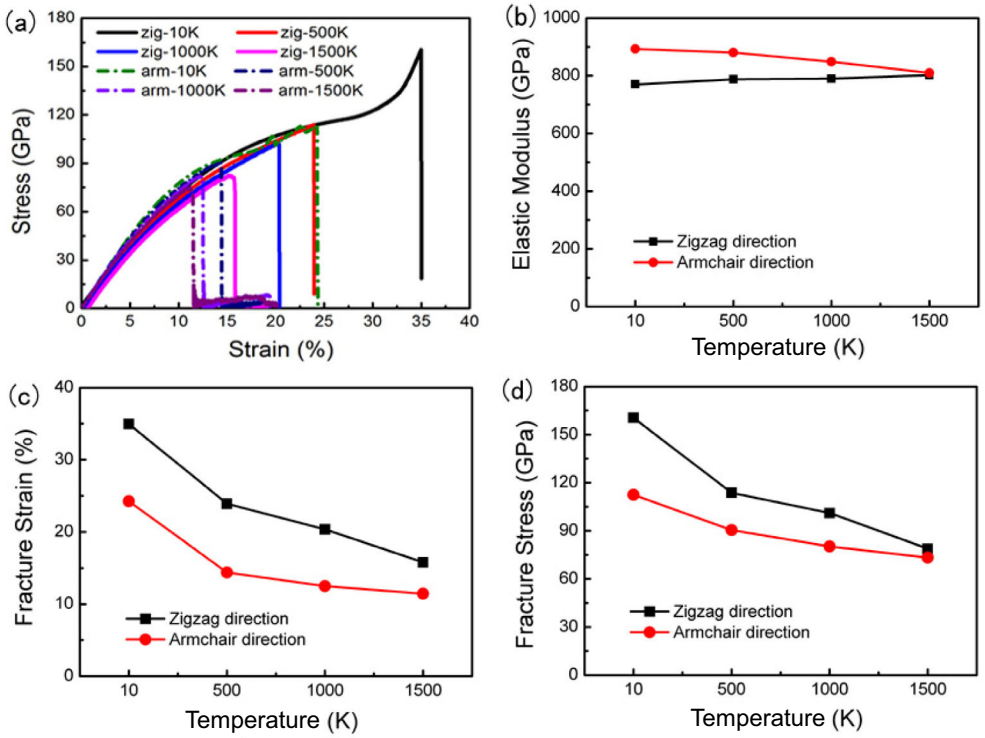

Fig. 2. (a) Stress-strain curves of single-crystal graphene sheets loaded along zigzag (denoted as "zig") and armchair (denoted as "arm") directions in the temperature range of 10 K–1500 K. (b)–(d) Elastic modulus, fracture strain, and fracture stress as a function of temperature.

sheets and a Poisson's ratio of 0.165 is used [28]. In the MD simulation, the time step is 1 fs and for each step, a strain increment of 10^{-5}–10^{-7} is applied corresponding to a strain rate in the range of 10^{10}–10^{8} s^{-1}. The temperature is between 10 K and 1500 K and controlled by the Nose'e-Hoover thermostat.

3 Results and discussion

3.1 Stress-strain curves of single-crystal graphene

Figure 2a shows the stress-strain curves of single-crystal graphene sheets loaded along the zigzag and armchair directions in the temperature range of 10 K to 1500 K. They all exhibit temperature- and orientation-dependent brittle fracture, and double-elastic deformation occurs in the graphene sheet loaded along the zigzag direction at 10 K as observed previously [29]. Figures 2b–2d display the elastic modulus, fracture strain, and fracture stress of the graphene sheets. The elastic modulus is between 800 GPa and 900 GPa and varies slightly with temperature. The values along the armchair direction are larger than those along the zigzag one similar to published results [13,23,30,31]. However, both the fracture stress and fracture strain decrease with temperature. For example, the fracture strain of the graphene sheets loaded along the zigzag direction decreases from 35% at 10 K to 18% at 1500 K by 49%, whereas the fracture stress drops from 160 GPa at 10 K to 90 GPa at 1500 K by 44%. The values along the zigzag direction are larger than those along the armchair direction, but the difference is reduced gradually with elevating temperature consistent with reported results [4,22]. The results of the ideal graphene sheets thus corroborate the calculation method as well as selected parameters.

3.2 Temperature effects

In nanocrystalline graphene sheets, the randomly-oriented grain domains may weaken the orientation dependence of the mechanical properties. A large number of grain boundaries with disordered and sparse atomic configuration will certainly enhance the activity of atoms and consequently, the mechanical behaviors become more sensitive to the temperature. Figures 3a–3c depict the stress-strain curves of the nanocrystalline graphene sheets with grain sizes of 6.17 nm, 3.7 nm and 2.06 nm, respectively and temperature dependent stress-strain curves are demonstrated. As shown in Figure 3d, the elastic modulus decreases with temperature due to the softening effect, but the reduction is less than 8%. It is considerable at temperature above 500 K and consistent with previous results [1]. Unexpectedly, the elastic modulus diminishes as the grain size decreases, but the fracture strain and fracture stress are almost independent of the grain size. This is completely different from the case found in nanocrystalline metals in which mechanical strength rather than elastic modulus is size dependent.

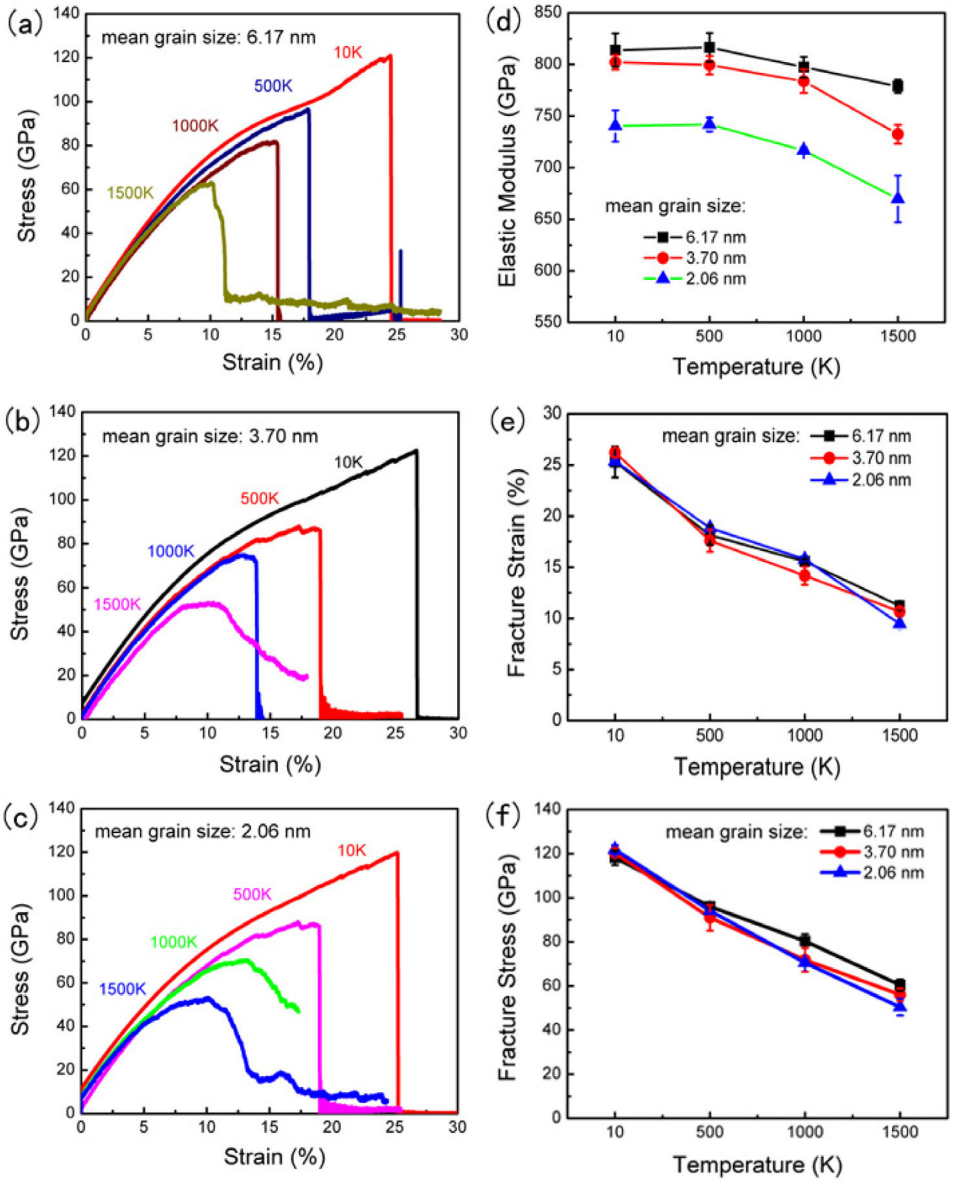

Fig. 3. Stress-strain curves of nanocrystalline graphene sheets with grain sizes of (a) 6.17 nm, (b) 3.70 nm, and (c) 2.06 nm tensile loaded at 10 K, 500 K, 1000 K, and 1500 K, respectively. (d)–(f) Elastic modulus, fracture strain, and fracture stress of the nanocrystalline graphene sheets.

Structurally, the grain boundaries become a principal component in the nanocrystalline graphene sheets and the individual behavior of atomic bonds in the grain boundaries dominates mechanical deformation. It is well known that grain boundaries can better accommodate bond rotation and reforming, thus leading to homogeneous bond length distributions. It is almost the same for all the samples and the fracture stress and fracture strain are size independent. However, the grain boundaries, as a low-elastic-modulus component, increase as the grain size decreases thereby resulting in reduced elastic modulus.

As shown in Figures 3a–3c, the stress at lower temperature increases with strain gradually initially but decreases sharply after a maximum stress indicative of brittle fracture in the nanocrystalline graphene sheets. However, above a critical temperature, the stress decreases from the maximum value gradually rather than abruptly. Plastic deformation seems to take place in the nanocrystalline graphene sheets at higher temperature. The smaller the grain size, the lower is the critical temperature. For example, the transition temperature is about 1500 K in the nanocrystalline graphene sheets with a grain size of 3.7 nm (Fig. 3b) but drops to 1000 K in the nanocrystalline graphene sheets with a grain size of 2.06 nm (Fig. 3c). Similar brittle-to-plastic transition is observed when the coverage of defects exceeds a critical value in graphene [32] and it is ascribed to a structural transition from crystalline to amorphous in the void content between 8% and 10% [33]. The results indicate that the brittle-to-plastic transition in the graphene sheets is closely related to the

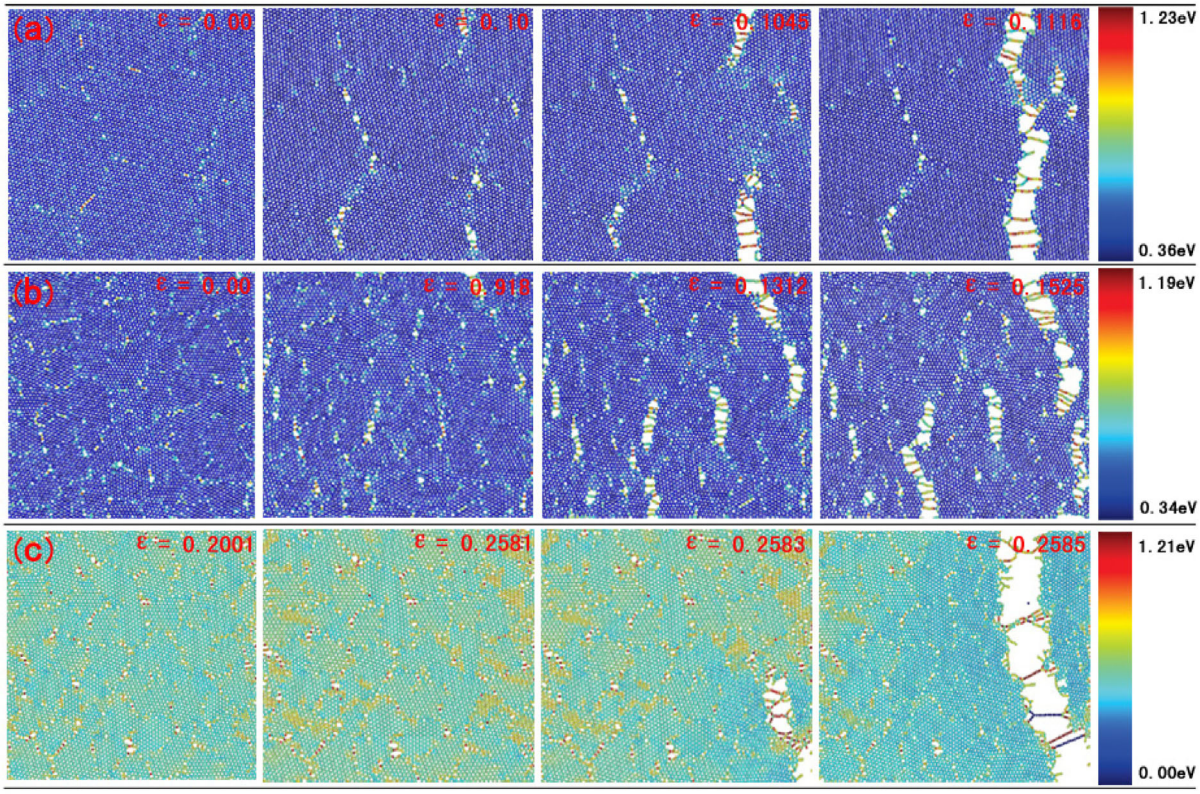

Fig. 4. Structure evolution of nanocrystalline graphene sheets: (a) grain size of 6.17 nm and loaded under a strain rate of 1.0×10^{-4} ps^{-1} at 1500 K, (b) grain size of 2.06 nm and loaded under a strain rate of 1.0×10^{-4} ps^{-1} at 1500 K, and (c) grain size of 2.06 nm and loaded under a strain rate of 1.0×10^{-4} ps^{-1} at 10 K.

disordered and sparse configuration of atoms locally. They can better accommodate bond rotation under stress and suppress collective bond breaking. It is more significant at high temperature because of increased structural disorder in the grain boundaries and hence, brittle fracture changes to plastic deformation above a critical temperature.

The maximum strain graphene sheets can sustain (Fig. 3e) and corresponding fracture stress (Fig. 3f) decrease with temperature indicating deteriorating ductility at high temperature, which is unexpected from nanocrystalline metals. This can be ascribed to the different deformation mechanisms. Plastic deformation in nanocrystalline metals is dominated by slipping and rotation of grains, which can be easily activated at a high temperature and so plastic deformation is enhanced [27,34]. However, fracture in graphene is dominated by the competition between breaking and rotation of covalent bonds. A high temperature accelerates bond breaking, leading to the reduced fracture strain and fracture stress. Figures 4a and 4b display the snapshots of the nanocrystalline graphene with grain sizes of 6.17 nm and 2.06 nm loaded at a strain rate of 1.0×10^{-4} ps^{-1} at 1500 K. The strain applied to the nanocrystalline graphene sheets is relaxed by the formation of voids in the grain boundaries and cracks are initiated there. In the graphene sheets with a larger grain size but a smaller volume of grain boundaries (Fig. 4a), the pre-existing voids grow larger and then expand along the weakest boundaries quickly, resulting in brittle fracture. On the other hand, in the graphene sheets with a smaller grain size but a larger volume of grain boundaries (Fig. 4b), the cracks bifurcate along different directions thus increasing the lifetime of the fracture. The carbon chains across the cracks in the grain boundaries are beneficial to the brittle-to-plastic transition. Figure 4c displays the snapshots of the graphene sheets 2.06 nm in grain size tensile loaded at 10 K for comparison showing the color distribution of the Von Mises shear strain. The shear strain is mainly localized at the grain boundaries in which the formation and growth of voids occur and brittle fracture ensues.

3.3 Strain rate effects

It has been reported that the strength of graphene sheets with tilt grain boundaries increases slightly with strain rate [35] and the tensile fracture strain varies linearly with the activation energy and temperature [18] and it can be quantitatively described by the Arrhenius-Zhurkov law [36]. Herein, by taking nanocrystalline graphene sheets with an average grain size of 2.06 nm as an example, the strain rate effects on the mechanical properties are studied. Figure 5 displays the stress-strain curves of the graphene sheets loaded at 10 K, 500 K, 1000 K, and 1500 K. The applied strain rates are 1.0×10^{-4} ps^{-1}, 5.0×10^{-4} ps^{-1}, 1.0×10^{-3} ps^{-1}, 2.5×10^{-3} ps^{-1},

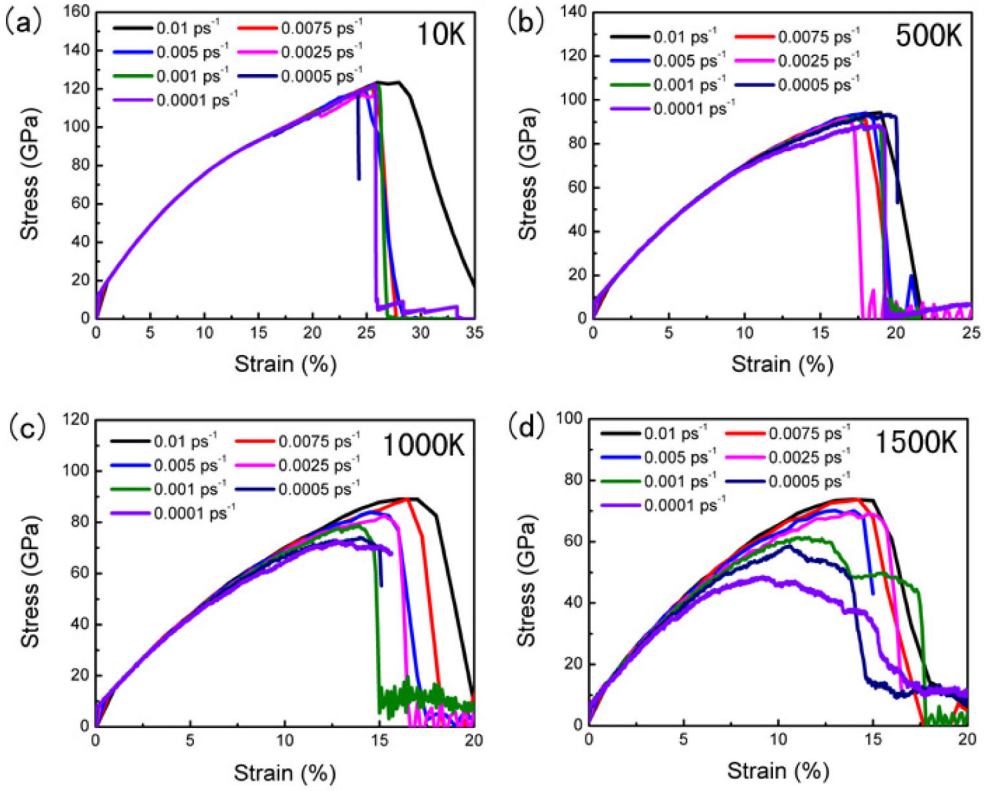

Fig. 5. Stress-strain curves of nanocrystalline graphene sheets with a grain size of 2.06 nm at (a) 10 K, (b) 500 K, (c) 1000 K and (d) 1500 K. The applied strain rate is between 1.0×10^{-2} ps^{-1} and 1.0×10^{-4} ps^{-1}.

7.5×10^{-3} ps^{-1}, and 1.0×10^{-2} ps^{-1}. The elastic modulus at low temperatures is nearly constant independent of the strain rate but decreases slightly with reducing stain rate at high temperature (Fig. 6a). As shown in Figure 5d, whether the nanocrystalline graphene sheets are plastic or brittle also depends on the strain rate. At small strain rates, bond rotation and rearrangement are easier thus benefiting flowing deformation and the aforementioned plastic deformation occurs. However, when the strain rate is increased, the relaxation time is too short for atomic bonds to rotate and rearrange under stress and hence, bond elongation and brittle fracture take place instead. This result in a plastic-to-brittle transition at a high strain rate, for instance, 2.5×10^{-3} ps^{-1} at 1500 K. Similar behavior has been observed from nanocrystalline Au thin films and CNTs [14,37]. The grain boundary mediated process becomes dominant at high temperature. Figures 6b and 6c show the fracture strain and stress as a function of strain rate. In the temperature range between 10 K and 500 K, both the fracture strain and fracture stress change slightly with strain rate, but it is different at above 1000 K when the fracture stress is strain rate independent. As addressed in the above section, at a low temperature, bond-breaking-induced brittle fracture dominates and depends only on bond elongation and it is thus insensitive to the strain rate. As the temperature rises above 1000 K, bond-rotation and rearrangement-dominant plastic deformation become possible and the synergistic effects of atoms are important. Hence, the mechanical deformation is sensitive to the strain rate. From the point of view of defects evolution, at a small strain rate, the relaxation time is long enough to promote bond rearrangement, vacancy coalescence, and crack propagation, thus giving rise to reduced fracture stress and fracture strain [38]. However, these processes are suppressed at a high strain rate and the defects tend to be homogenously distributed resulting in increased fracture stress. Brittle fracture dominates at above a critical strain rate and the fracture stress becomes nearly strain rate independent. This leads to the two stages of the strain rate dependent behaviors as illustrated in Figures 6b and 6c.

Generally, in nanocrystalline metals, the strain-rate-dependent mechanical behavior is determined by the dislocation activity, grain boundary diffusion, and lattice diffusion [39] as $\sigma = K\dot{\varepsilon}^m$, in which σ is the yield strength, $\dot{\varepsilon}$ is the strain rate, K is a constant, and m is the strain rate sensitivity exponent. This process can be extrapolated to nanocrystalline graphene sheets but the yield strength should be replaced by the fracture stress. As shown in Figure 7, the m values are smaller than 0.03 at temperature lower than 500 K but are between 0.05 and 0.10 at high temperature and also change with the temperature considerably. This indicates that mechanical deformation of the nanocrystalline graphene sheets is more sensitive to the strain rate at high temperature. As stated in reference [31], 5-7 topological defects are similar to the edge dislocations in metals. Hence, the concept "dislocation" has been widely adopted to describe and interpret the

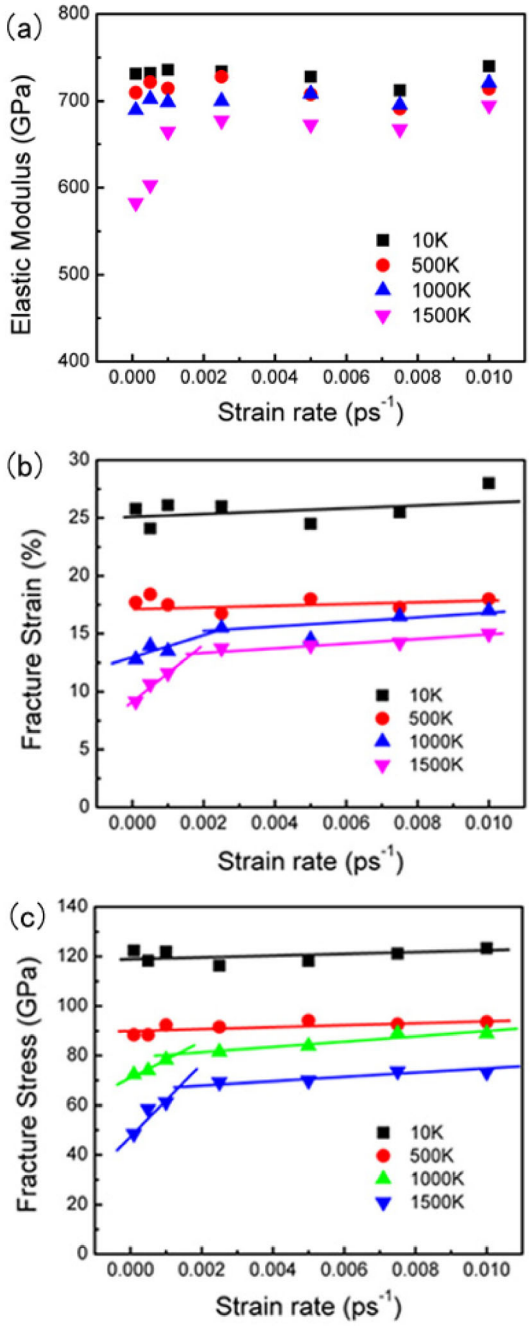

Fig. 6. (a) Elastic modulus, (b) fracture strain, (c) fracture stress as a function of strain rates. The curves for (b) and (c) can be divided into two stages according to the slopes indicating the plastic-to-brittle deformation transformation.

plastic deformation in graphene and carbon nanotubes (CNTs) [31,40,41]. So the deformation behaviors of the nanocrystalline graphene sheets are discussed according to the classic dislocation theory, in which the activation volume V can be calculated by [42]:

$$V = \sqrt{3}kT\left(\frac{\partial \ln \dot{\varepsilon}}{\partial \sigma}\right), \tag{2}$$

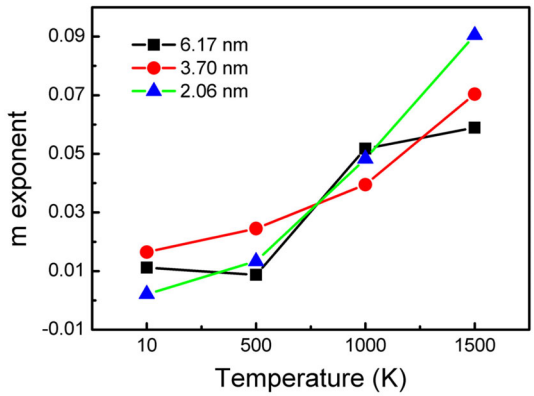

Fig. 7. m exponent of nanocrystalline graphene sheets with grain sizes of 6.17 nm, 3.70 nm and 2.06 nm as a function of temperature.

where k is Boltzmann's constant, T is the absolute temperature, σ is the fracture stress, and $\dot{\varepsilon}$ is the strain rate. The calculated activation volumes at 1500 K are $5.71b^3$ and $3.45b^3$ for the nanocrystalline graphene sheets loaded at a strain rate smaller than 1.0×10^3 ps^{-1} and larger than that value, respectively, in which b is the Burgers vector of (1,0) dislocation [31] and $|b| = 2.46$ Å. Apparently, the activation volume is in the atomic scale, that is, the deformation is dominated by the local atomic behavior in GBs. Moreover, the larger the strain rate is, the smaller the activation volume is. This is consistent with our conventional sense. All this indicates the validity of the classic dislocation theory in studying the deformation of graphene sheets, at least semi-quantitatively.

4 Conclusion

The deformation behavior and mechanical properties of 2D graphene systems are crucial to their applications to flexible devices and composite materials. In nanocrystalline graphene sheets, there are many grain boundaries with disordered and sparse atomic configurations and as a result, nanocrystalline graphene sheets are expected to possess temperature and strain-rate dependent deformation behavior and mechanical properties. The phenomenon is investigated by molecular dynamics simulation. The elastic modulus decreases with temperature as a result of softening, but the reduction is smaller than 8% nearly independent of the strain rate. Plastic deformation appears to take place in the nanocrystalline graphene sheets at higher temperature but the ductility deteriorates unexpectedly. This can be ascribed to accelerated bond breaking. Whether the nanocrystalline graphene sheets are plastic or brittle also depends on the strain rate. At low strain rates, it is easier for bonds to rearrange, vacancies to coalesce, and cracks to propagate in grain boundaries and plastic deformation with a larger activation volume occurs. However, when the strain rate is increased, the relaxation time is too short for atomic bonds to rotate and rearrange under stress and, bond elongation and brittle fracture with a smaller activation volume takes place.

This results in a plastic-to-brittle transition at a large strain rate.

This work was jointly supported by Key Project of Chinese National Programs for Fundamental Research and Development (Grant No. 2010CB631002), National Natural Science Foundation of China (Grant Nos. 51271139, 51302162, 51471130, 51171145), the Natural Science Foundation of Shaanxi Province (2013JM6002), and Fundamental Research Funds for the Central Universities and Guangdong – Hong Kong Technology Cooperation Funding Scheme (TCFS) GHP/015/12SZ.

Fei Ma and Kewei Xu designed the research work, Zhi Yang, Yuhong Huang and Yunjin Sun carried out the modeling, Fei Ma, Zhi Yang, Yuhong Huang and Yunjin Sun analyzed the simulation results, Zhi Yang, Yuhong Huang, Fei Ma, Yunjin Sun, Kewei Xu and Paul K. Chu prepared the manuscript.

References

1. K. Novoselov et al., Nature **438**, 197 (2005)
2. K.I. Bolotin et al., Solid State Commun. **146**, 351 (2008)
3. A.A. Balandin et al., Nano Lett. **8**, 902 (2008)
4. C. Lee, X. Wei, J.W. Kysar, J. Hone, Science **321**, 385 (2008)
5. J. Van den Brink, Nat. Nanotechnol. **2**, 199 (2007)
6. A.C. Neto, F. Guinea, N. Peres, K.S. Novoselov, A.K. Geim, Rev. Mod. Phys. **81**, 109 (2009)
7. S. Bae et al., Nat. Nanotechnol. **5**, 574 (2010)
8. R. Nair et al., Science **320**, 1308 (2008)
9. D. Reddy, L.F. Register, G.D. Carpenter, S.K. Banerjee, J. Phys. D **44**, 313001 (2011)
10. E. Huitema, Inf. Display **28**, 6 (2012)
11. P. Zhang, P.E. Lammert, V.H. Crespi, Phys. Rev. Lett. **81**, 5346 (1998)
12. H. Gwon et al., Energy Environ. Sci. **4**, 1277 (2011)
13. F. Ma, Y. Sun, D. Ma, K. Xu, P.K. Chu, Acta Mater. **59**, 6783 (2011)
14. K.S. Novoselov et al., Science **306**, 666 (2004)
15. S. Stankovich et al., Nature **442**, 282 (2006)
16. R. Grantab, V.B. Shenoy, R.S. Ruoff, Science **330**, 946 (2010)
17. S.S. Terdalkar, S. Huang, H. Yuan, J.J. Rencis, T. Zhu, S. Zhang, Chem. Phys. Lett. **494**, 218 (2010)
18. C. Wei, K. Cho, D. Srivastava, Phys. Rev. B **67**, 115407 (2003)
19. H. Zhao, N. Aluru, J. Appl. Phys. **108**, 064321 (2010)
20. K. Min, N. Aluru, Appl. Phys. Lett. **98**, 013113 (2011)
21. M.C. Wang et al., J. Nano Res. **23**, 43 (2013)
22. J.H. Warner, E.R. Margine, M. Mukai, A.W. Robertson, F. Giustino, A.I. Kirkland, Science **337**, 209 (2012)
23. M. Wang, C. Yan, L. Ma, N. Hu, M. Chen, Comput. Mater. Sci. **54**, 236 (2012)
24. A. Carpio, L.L. Bonilla, F. de Juan, M.A. Vozmediano, New J. Phys. **10**, 053021 (2008)
25. D.W. Brenner, O.A. Shenderova, J.A. Harrison, S.J. Stuart, B. Ni, S.B. Sinnott, J. Phys: Condens. Matter **14**, 783 (2002)
26. O.A. Shenderova, D.W. Brenner, A. Omeltchenko, X. Su, L.H. Yang, Phys. Rev. B **61**, 3877 (2000)
27. J. Schiøtz, F.D. Di Tolla, K.W. Jacobsen, Nature **391**, 561 (1998)
28. X. Wei, B. Fragneaud, C.A. Marianetti, J.W. Kysar, Phys. Rev. B **80**, 205407 (2009)
29. Y. Sun, Y. Huang, F. Ma, D. Ma, T. Hu, K. Xu, Mater. Sci. Eng. B **180**, 1 (2014)
30. Z. Xu, M.J. Buehler, J. Phys: Condens. Matter **22**, 485301 (2010)
31. O.V. Yazyev, S.G. Louie, Phys. Rev. B **81**, 195420 (2010)
32. L. Xu, N. Wei, Y. Zheng, Nanotechnol. **24**, 505703 (2013)
33. C. Carpenter, D. Maroudas, A. Ramasubramaniam, Appl. Phys. Lett. **103**, 013102 (2013)
34. R. Valiev, Nat. Mater. **3**, 511 (2004)
35. L. Yi, Z. Yin, Y. Zhang, T. Chang, Carbon **51**, 373 (2013)
36. A. Iskandarov, S. Dmitriev, Techn. Phys. Lett. **39**, 185 (2013)
37. T. Albrecht, H. Mizes, J. Nogami, Si. Park, C. Quate, Appl. Phys. Lett. **52**, 362 (1988)
38. Y.J. Sun, Y.H. Huang, F. Ma, D.Y. Ma, T.W. Hu, K.W. Xu, Mater. Sci. Eng. B **180**, 1 (2014)
39. J. Chen, L. Lu, K. Lu, Scr. Mater. **54**, 1913 (2006)
40. M.B. Nardelli, B.I. Yakobson, J. Bernholc, Phys. Rev. Lett. **81**, 4656 (1998)
41. K. Suenaga, H. Wakabayashi, M. Koshino, Y. Sato, K. Urita, S. Iijima, Nat. Nanotechnol. **2**, 358 (2007)
42. R.J. Asaro, S. Suresh, Acta Mater. **53**, 3369 (2005)